

Structural Analysis and Characteristics of Deformed and Heat-treated Al-Fe-Ni-Mg

M. Husna Al Hasa^a, Wisnu Ariadi^b, Masrukan^a, Kemal Maulana Alhasa^c, Usman Sujadi^a,
Ratih Langenati^a, Djati Handoko^d, Dede Djuhana^d

^a Research Center for Nuclear Fuel Cycle and Radioactive Waste Technology, National Research and Innovation Agency, Indonesia

^b Research Center for Advanced Material, National Research and Innovation Agency, Indonesia

^c Research Center for Environmental and Clean Technology, National Research and Innovation Agency, Indonesia

^d Department of Physics, Faculty of Mathematics and Natural Sciences (FMIPA), Universitas Indonesia, Depok, Indonesia

Corresponding author: *mhalhasa@yahoo.com

Abstract—The study of aluminum alloys (Al-Fe-Ni-Mg – Aluminum – Iron – Nickel - Magnesium) was carried out to develop high-density research reactor fuel cladding materials. Aluminum alloy as a fuel cladding undergoes a deformation process and heat treatment above the recrystallization temperature. Deformation and heat treatment will change in structure, microstructure, and mechanical properties. This study aims to determine aluminum alloy's phase structure, microstructure, and hardness after deformation and heat treatment. Phase structure analysis was carried out based on the X-ray diffraction pattern method. Observation of microstructural changes was carried out by metallographic-optical Scanning Electron Microscopy (SEM), and elemental analysis of alloying phase compounds was carried out by Energy Dispersive Spectroscopy – Scanning Electron Microscopy (EDS-SEM). The Vickers hardness tester tested the hardness properties of the material. The analysis of the x-ray diffraction patterns showed a tendency to form α and θ (Fe-Al₃) phases in the alloy. The metallographic-optical observations showed that the microstructure changed with an increasing heating time of 3 hours. The microstructure tends to form an enlarged equiaxial grain structure with a long heating time. The results of testing the hardness properties of the Al-Fe-Ni-Mg alloy showed an increase of around 163 HV after undergoing the deformation process and heating treatment at 500 °C to 3 hours of heating time decreased around 86 HV. The changes in hardness properties of the Al-Fe-Ni-Mg alloy appear to align with changes in the microstructure. The deformation process and heat treatment impact the mechanical characteristics and microstructure of Al-Fe-Ni-Mg.

Keywords—Deformation; heat treatment; mechanical properties; phase structure; Al-Fe-Ni-Mg alloy.

Manuscript received 12 Sep. 2023; revised 14 Nov. 2023; accepted 25 Feb. 2024. Date of publication 31 Aug. 2024.
IJASEIT is licensed under a Creative Commons Attribution-Share Alike 4.0 International License.



I. INTRODUCTION

In nuclear plants, aluminum alloys have been extensively used, particularly as structural materials for the cladding of fuel elements [1]. Due to the requirement for the development of high-density fuel, aluminum-based cladding structural materials have been extensively developed in several nations, including Indonesia. Aluminum alloys have been explored for use as cladding structural materials since they have substantially higher strength, thermal qualities, and relatively high corrosion resistance [2]. Based on previous studies, the mechanism of the synthesis process can be used to enhance the strength features of aluminum alloys [3]. Several metal components, including Al, Fe, Ni, and Mg, are combined during the synthesis process to enhance the properties of

metals [3], [4]. Numerous studies have shown that various mechanisms, including strain hardening, solid solution, and second-phase formation, can enhance the physical properties of metals [4], [5], [6].

Aluminum alloys are subjected to heating and deformation processes during the manufacturing process. fuel cladding will probably alter in terms of its phase structure, hardness, thermal characteristics, and phase transformation throughout the heating process at high temperatures [6]. Heat treatment at high temperatures will probably initiate the diffusion reaction of intermetallic metal complexes Al with Fe, Ni, and Mg [6], [7]. The diffusion process in heat treatment tends to yield metal compounds of phase θ , phase κ , phase τ , and other compounds [7],[8]. Below 652 °C, the alloy region with a composition of 0.04–37% Fe is where the phase θ compound (Fe-Al₃) starts forming [9]. This phase compound, designated

$L \rightarrow \alpha + \theta$, is produced by the transition of Al and Fe alloys after the eutectic phase reaction. Fe concentrations in alloys above the solid solubility limit of 0.04% tend to generate phase- α compounds [9],[10]. In the meantime, the phase κ compound begins to form in the range of Ni's weight of about 0.04–42% and the temperature below 640 °C. Al and Ni alloys undergo a transformation that yields the phase κ compound $L \rightarrow \alpha + \kappa$ after following the eutectic phase reaction. Furthermore, phase κ (NiAl_3) will form if the Ni content in the alloy reaches the solid soluble limit above 0.04%. Given that the amount of Ni in the alloy has been shown to have a significant impact on the magnitude of phase κ . When the temperature reaches 652 °C and the Fe concentrate is around 1.8%, the eutectic phase reaction for aluminum and iron alloys begins. This reaction will produce the $\text{Al} + \text{Fe} + \text{Al}_3 \alpha + \theta$ solid phase, where the α phase has a solid solubility limit at Fe levels of around 0.04%. This reaction yields an Al-Fe-Ni metal alloy with a polytropic and anisotropic structure that is monoclinic and orthorhombic. A chemical reaction that forms the phase (Al_9FeNi) is also conceivable at a temperature of 640 °C, according to studies conducted by [11], [12].

The formation of the phase structure in the alloy has a considerable influence on the strength and corrosion resistance of Al-Fe-Ni-Mg structural materials [13],[14]. In this case, the number of combiners and combining components in the alloy has influenced the phase information. The formation of phases in metal alloys is possible if the composition consists of two or more elements with atomic radius differences significant enough to create a solid solution as one of the phases. Furthermore, the phases formed differ in their characteristics, lattice sizes, crystal shapes, and liquid points. The atomic sizes, interatomic distances, and crystal shapes of Al, Fe, Ni, and Mg can vary. Al metal has a crystal structure like an FCC (Face Centered Cubic) unit cell with lattice parameters and an interatomic distance of 4.0496 and 2.8635, respectively. Fe metal has a BCC (Body-Centered Cubic) crystal structure with lattice parameters 2.8664 and an interatomic distance of 2.4823. In contrast, Ni metal has an FCC unit with a lattice Size of 3.52338 and an interatomic distance of 2.4919.

The phase structure, hardness, thermal, and corrosion properties will be examined to understand Al-Fe-Ni-Mg as cladding structural materials better. This study's results can help develop materials for cladding nuclear fuel elements.

II. MATERIALS AND METHOD

Through a synthesis process, two or three components combined with aluminum as the primary element to form aluminum alloys. The composition levels of each metal 1wt.%, 1wt.%, 1%wt., and 1wt % for Fe, Ni, and Mg, respectively were used to calculate the weight of the material. Furthermore, aluminum, Ferro, nickel, and magnesium metals were weighed using a digital balance at predefined levels. Based on the composition of the eutectic alloy, the weight of the ferro and nickel powders with the aluminum metal was adjusted proportionally. Al-Fe and Al-Ni metal alloys are formed from this mixture of metals with eutectic alloy composition by melting them at temperatures higher than their eutectic point temperature.

TABLE I
THE SUMMARY OF ELEMENTS' COMPOSITION

Elements	Fe	Ni	Mg
Weight (%)	1wt.	1wt.	1wt.

The smelting of aluminum metal with approximate Al-Fe, Al-Ni, and Al-Mg alloy compositions is performed at 800°C. This melting procedure yields Al-Fe-Ni-Mg alloy plates. Furthermore, the Al-Fe-Ni-Mg plate specimens were homogenized at 500°C for 13 hours. Following the homogenization process, Al-Fe-Ni-Mg plate specimens are gradually deformed by rolling till the reduction is around 87 %. The deformed Al-Fe-Ni-Mg plate from the rolling process is then subjected to a second heating process at 500°C for three periods, including 1, 2, and 3 hours. Furthermore, the Al-Fe-Ni-Mg plates were analyzed, tested, observed, and measured.

The Vickers hardness tester was used to assess the hardness of Al-Fe-Ni-Mg specimens, and an x-ray diffractometer was used to analyze the phase structure of Al-Fe-Ni-Mg alloys based on x-ray diffraction patterns. Metallographic-optical and SEM microscopy were used to make microstructural observations. A Philip-type PW1710 x-ray diffractometer (XRD) was used to measure the quality and amount of phases present in the samples. In contrast, EDS was used to observe the elemental analysis of metal compounds. With a continuous-scan mode, step size of 0.02°, and time per step of 0.5 seconds, an x-ray beam with a wavelength of $\lambda = 1.5406$ was used to measure the sample's diffraction pattern. The law Breeg is used to determine diffraction angel as shown in equation 1. The computer program RIETAN (Rietveld Analysis) 1994 was used to examine the x-ray diffraction profiles [15].

$$n\lambda = 2d \sin \theta \quad (1)$$

where n and λ are constantan in integer unit and wavelength of x-ray, respectively. On the other hand, d is the spacing of the crystal layers, and θ is the incident layer.

III. RESULT AND DISCUSSION

Fig. 1 shows the outcomes of x-ray diffraction measurements on Al-Fe-Ni-Mg plates that had been rolled and heated at 500 °C for 1, 2 and 3 hours. As observed in Fig. 1, there are multiple peaks with identical X-ray diffraction patterns that are located at diffraction angles of approximately $2\theta = 38^\circ, 44^\circ, 65^\circ, 78^\circ, \text{ and } 82^\circ$. In contrast to the original deformed plate, there are splitting peaks at $2\theta = 38^\circ$ and 44° diffraction angles. According to phase identification results, identical diffraction peaks become visible due to the following overlaps with the diffraction pattern of the cubically structured Al phase, which has space group $Fm\bar{3}m$ (225) and lattice parameters $a = b = c = 4.0496 \text{ \AA}$ [16]. In the meantime, the splitting peaks probably contain more than one phase, including the Al phase or the solid solution Al phase. The crystal structures of the first and second Al phases are identical, but substituting Fe, Ni, and Mg atoms has changed their lattice properties. The results of the phase identification indicate that the first phase, which includes the planes (111), (200), (220), (311), and (222), is at diffraction angles $2\theta = 38.52^\circ, 44.69^\circ, 65.42^\circ, 78.51^\circ, \text{ and } 82.72^\circ$, respectively. The

(111) and (200) planes for the second phase, which is considered to be identical to the first phase, are at diffraction angles $2\theta = 38.98^\circ$ and 45.17° , respectively, while the (220), (311), and 222 planes have been found to coincide with the Al phase.

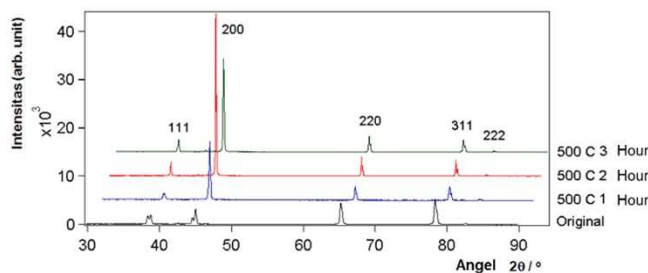


Fig. 1 X-ray diffraction pattern of Al-Fe-Ni-Mg plate

The Dirac factor influences the confusion of peaks at high angles according to the rules of X-ray diffraction patterns. The splitting of peaks becomes invisible as high angles increase. Furthermore, the impurity phase has a comparatively low actual intensity compared to the Al or Al solid solution phases. Therefore, the mass fraction is expected to be low. As a result, the impurity phase in this study is negligible. According to the reference x-ray diffraction pattern, the Al phase powder will have its highest peak when it is in the Miller index plane (111), followed by (200), (311), (220), and (222). However, the deformed Al-Fe-Ni-Mg sample shows its highest peak when it is at the Miller index (311), followed by (220), (200), (111), and (222). This is owing to the deformation process, which resulted in a preferred orientation in the (311), (220), and (200) planes.

The original deformed Al-Fe-Ni-Mg sample's x-ray diffraction pattern results after refining are shown in Fig. 2.

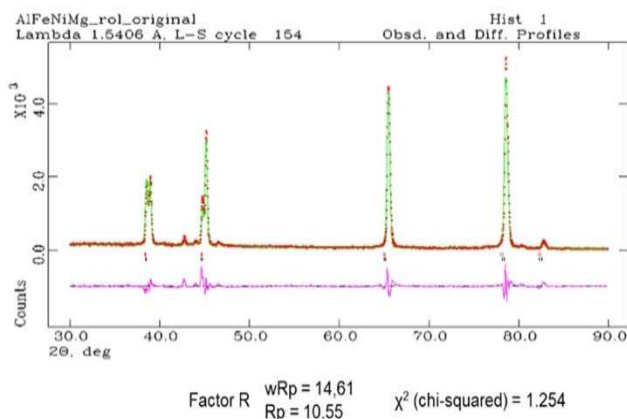


Fig. 2 Refinement of X-ray diffraction pattern of original Al-Fe-Ni-Mg

Based on the results of the refinement on the original deformed Al-Fe-Ni-Mg sample, it has a very good x-ray diffraction pattern where the values of the R factor for wRp and Rp (criteria of fit), and χ^2 (goodness of fit) are 14.61, 10.55, and 1.254, respectively. These values meet the requirements, where the R factor and χ^2 factor should be relatively small and less than 1.3, respectively [15],[16]. Moreover, the structural properties of the Al-Fe-Ni-Mg original deformation and the mass percent of each sample are shown in Tables 2 and 3.

TABLE II
STRUCTURE PARAMETERS OF ORIGINAL AL-FE-NI-MG

space group: F m -3 m (225), Crystal system: Cubic [16]							
Lattice parameters of AlMg				Lattice parameters of Al-Fe-Ni Phase:			
Phase: $a = b = c = 4.0542(1) \text{ \AA}$, $\alpha = \beta = \gamma = 90^\circ$				Phase: $a = b = c = 4.599(7) \text{ \AA}$, $\alpha = \beta = \gamma = 90^\circ$			
$V = 66.640(6) \text{ \AA}^3$ and $\rho = 2.559 \text{ gr.cm}^{-3}$				$V = 66.92(3) \text{ \AA}^3$ and $\rho = 3.222 \text{ gr.cm}^{-3}$			
Atom	neq	g	n	x	y	z	B
Al	2	1.0	2.0	0.0	0.0	0.0	1.0

TABLE III
THE MASS FRACTION CONTAINED IN THE ORIGINAL AL-FE-NI-MG

No.	Phase	Mass fraction (% Weight)
1.	AlMg (solid solution)	70,22
2.	Al-Fe-Ni (solid solution)	29,78

According to the structural parameter data analysis shown in Table 1, the Al, Al-Mg, and Al-Fe-Ni phases have a lattice parameter, a unit cell volume, an atomic density of 4.0496 \AA , 66.41 \AA^3 , and 2.697 gr.cm^{-3} , $4.0542(1)\text{\AA}$, $66.640(6)\text{\AA}^3$, and 2.559 gr.cm^{-3} , and $4.599(7) \text{ \AA}$, $66.92(3) \text{ \AA}^3$, and 3.222 gr.cm^{-3} , respectively. Further investigation of the x-ray diffraction pattern and an elementary examination of the original Al-Fe-Ni-Mg sample reveal the formation of solid solution phases of AlMg and Al-Fe-Ni with mass fraction contents of 70.22% and 29.78%, respectively, as shown in Table 2. On the other hand, a summary of the cationic distribution of each phase in the sample, including AlMg and Al-Fe-Ni, is shown in Table 4.

TABLE IV
EACH PHASE'S CATIONIC DISTRIBUTION IN THE ORIGINAL AL-FE-NI-MG

Sample	Cationic distributions				
	AlMg phase		Al-Fe-Ni phase		
	Al	Mg	Al	Fe	Ni
Content (at %)	98.87	1.13	91.27	5.01	3.72
Content (wt %)	98.98	1.02	83.17	9.45	7.38
Composition of refined	Al _{0.989} Mg _{0.011}		Al _{0.913} Fe _{0.05} Ni _{0.037}		
Composition of element analysis	Al _{0.985} Mg _{0.015}		Al _{0.943} Fe _{0.022} Ni _{0.036}		

The formation of the AlMg solid solution phase has been recognized based on changes in the significant structural properties of the original Al phase. It is shown that Al atoms have partially substituted for Mg atoms, resulting in a more significant gap between lattices. A similar process happens if several Al atoms are substituted with Fe and Ni atoms, causing the distance between the lattice to increase.

However, there is a difference in atomic density, with the Al-Mg phase having a substantially lower atomic density than the Al phase. In the meantime, the Al-Fe-Ni phase has a substantially higher atomic density than the Al phase. The reduced atomic density of the Al-Mg phase is attributable to the properties of the Mg atom itself, as Mg atoms have a relatively low atomic density of 1.74 gr.cm^{-3} compared to the atomic density of Al of 2.697 gr.cm^{-3} . It leads to a decrease in the Al-Mg phase's atomic density. On the other hand, the atomic density of Fe and Ni is quite high, at 7.86 gr.cm^{-3} and 8.9 gr.cm^{-3} , respectively, which will lead to an increase in the atomic density of the Al-Fe-Ni phase.

Furthermore, based on the findings of the elementary test on the original Al-Fe-Ni-Mg sample, there appear to be two distinct color variances, as illustrated in Fig. 3. This indicates that the substance being looked into contains more than one phase. Fig. 3 shows granular particles in light (white) and dark (grey) colors based on the EDS analysis, indicating that the light (white) portions are classified as Al, Fe, and Ni elements. In contrast, the dark (grey) parts are identified as Al and Mg elements. It indicates that the alloying elements Fe, Ni, and Mg have diffused as replacements or interstitials in the Al phase, resulting in a densely saturated Al solution phase [17],[18],[19]. The elementary analysis result is shown in Figs. 4 and 5.

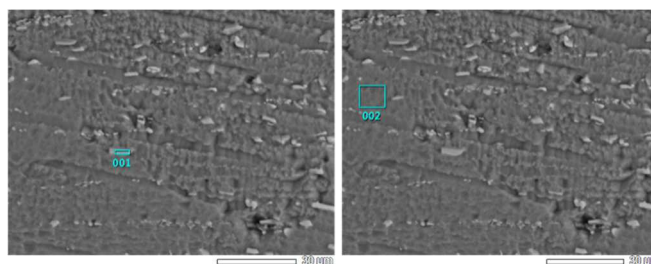


Fig. 3 Electron backscatter image of the original Al-Fe-Ni-Mg

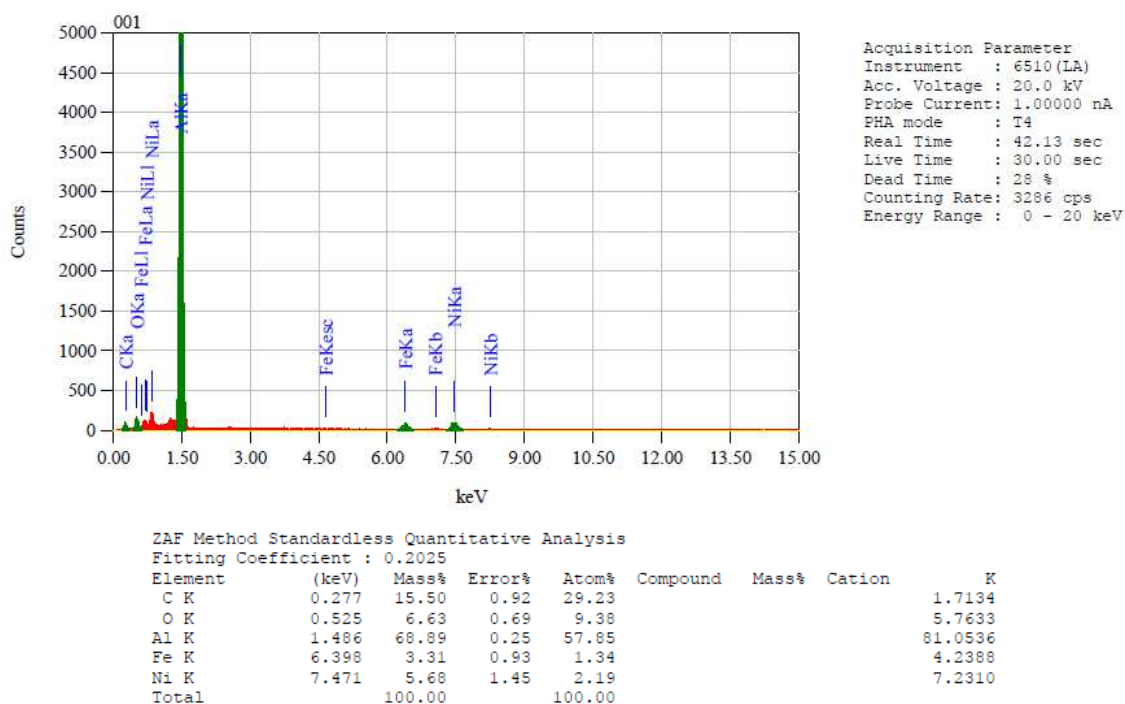


Fig. 4 The results of an elementary analysis of color spot code-001 in the original Al-Fe-Ni-Mg

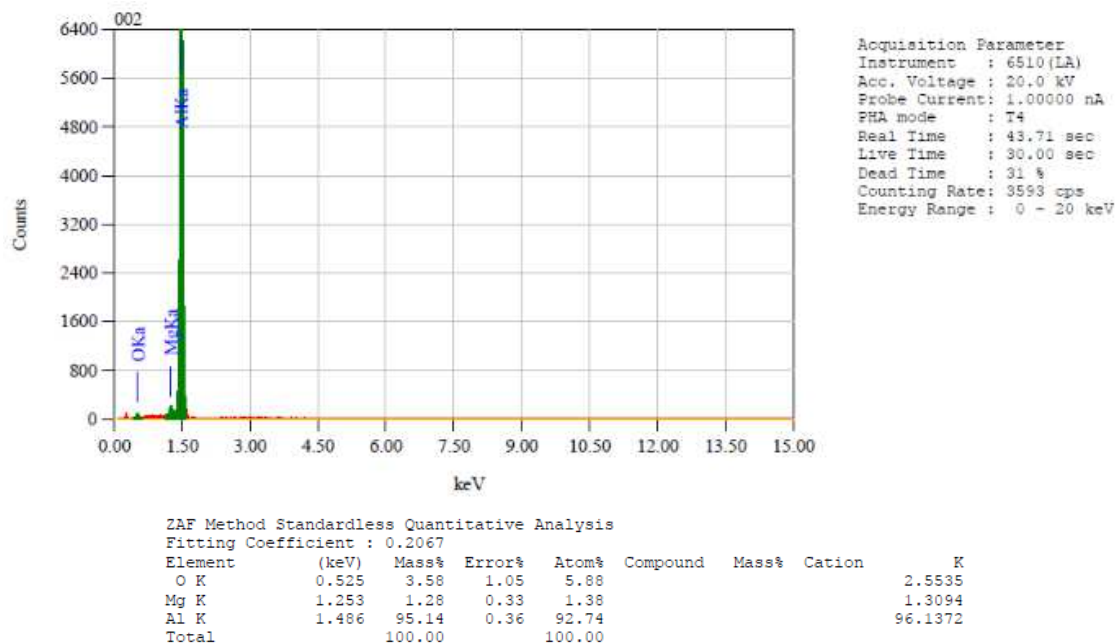
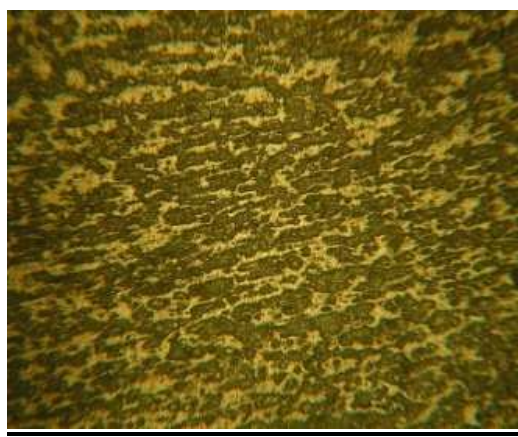


Fig. 5 The results of an elementary analysis of color spot code-002 in the original

The resulting solid solution phase influences changes in the Al phase's lattice properties, which tend to rise. The rise in lattice parameters causes inter-atomic stress, which causes changes in the metal's mechanical characteristics. Furthermore, due to plastic deformation, the microstructure appears flat-elongated, and the crystal orientation tends to point in a specific direction, as illustrated in Fig. 6. Metal crystals with a specific orientation of cells will have higher metal hardness qualities. The increase happens due to the varied orientation of each grain, which causes the orientation of the slip plane on each grain to vary. As a result, dislocation movement will be inhibited and hindered, requiring more power to carry out dislocation movement. Grain boundaries in the grain structure act as impediments to dislocation migration. Because there are more impediments, the more grain boundaries there are, the heavier the dislocation movement [20],[21],[22],[23].



20 μm

Fig. 6 Deformed grain microstructure of Al-Fe-Ni-Mg

It has previously been explained that the occurrence of the highest peak based on the Miller index in the Al-Fe-Ni-Mg sample differs from the reference Al phase powder X-ray diffraction pattern due to the deformation of the original Al-Fe-Ni-Mg sample. It could happen since rolling deformation leads to a preferred orientation in the (200), (311), (220), and (200).

However, how much of the orientation in the Al-Fe-Ni-Mg sample will be looked into based on the refinement findings of the x-ray diffraction patterns shown in Figs. 7, 8, and 9 with heat treatment at 500 °C for 1 hour, 2 hours, and 3 hours, respectively.

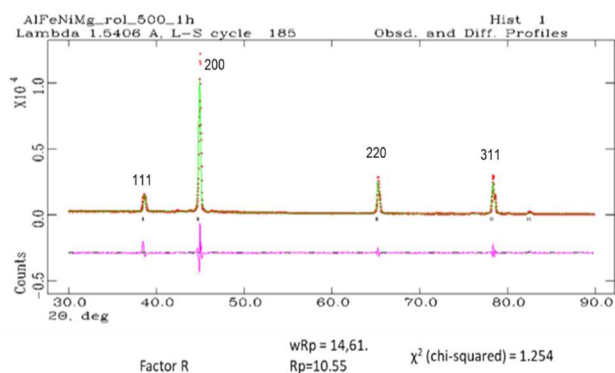


Fig. 7 Refinement of the x-ray diffraction pattern of Al-Fe-Ni-Mg after 1 hour of heating

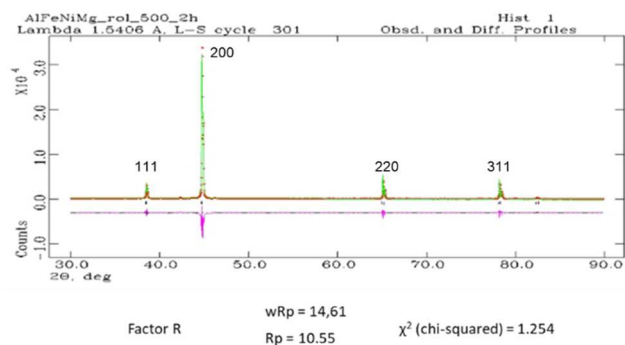


Fig. 8 Refinement of the x-ray diffraction pattern of Al-Fe-Ni-Mg after 2 hours of heating

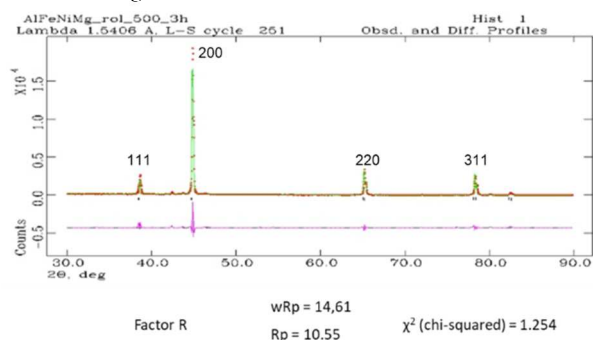


Fig. 9 Refinement of the x-ray diffraction pattern of Al-Fe-Ni-Mg after 3 hours of heating

In the meantime, the outcomes of refinement during the heating process of 1 hour, 2 hours, and 3 hours for each structural parameter are shown in Tables 5-7, respectively. In Figs. 7, 8 and 9 show a change in the Al-Fe-Ni-Mg X-ray diffraction pattern after heating for up to 3 hours. The Al-Fe-Ni-Mg X-ray diffraction pattern resulting from heating for 1 hour showed the highest peaks at the Miller index (200), then (311), (220), (111) and (222). 2 hours of heating, the highest peaks are at the Miller index (200), then (220), (311), (111) and (222). Meanwhile, the highest peak of 3-hour warming is at the Miller index (200) then (220), (311), (111) and (222). It indicates a change in crystal orientation and atomic position in the crystal lattice structure, which has an impact on changes in the phase, microstructure and properties of the material [24], [25], [26], [27].

TABLE V
STRUCTURAL PARAMETERS OF AN AL-FE-NI-MG AFTER 1 HOUR OF HEATING

Space group: F m -3 m (225), Crystal system: Cubic (Wyckoff)	
Lattice parameters of AlMg Phase: $a = b = c = 4.0542(1)$ Å , $\alpha = \beta = \gamma = 90^\circ$ $V = 66.640(6) \text{ \AA}^3$ and $\rho = 2.559 \text{ gr.cm}^{-3}$	Lattice parameters of Al-Fe-Ni Phase: $a = b = c = 4.599(7) \text{ \AA}$, $\alpha = \beta = \gamma = 90^\circ$ $V = 66.92(3) \text{ \AA}^3$ and $\rho = 3.222 \text{ gr.cm}^{-3}$

TABLE VI
STRUCTURAL PARAMETERS OF AN AL-FE-NI-MG AFTER 2 HOUR OF HEATING

Space group: F m -3 m (225) Crystal system: Cubic (Wyckoff)	
Lattice parameters of AlMg Phase: $a = b = c = 4.0542(1)$ Å , $\alpha = \beta = \gamma = 90^\circ$ $V = 66.640(6) \text{ \AA}^3$ and $\rho = 2.559 \text{ gr.cm}^{-3}$	Lattice parameters of Al-Fe-Ni Phase: $a = b = c = 4.599(7) \text{ \AA}$, $\alpha = \beta = \gamma = 90^\circ$ $V = 66.92(3) \text{ \AA}^3$ and $\rho = 3.222 \text{ gr.cm}^{-3}$

TABLE VII
THE STRUCTURAL PARAMETERS OF AN AL-FE-NI-MG AFTER 3 HOUR
OF HEATING

Space group: Fm-3m (225)	Crystal system: Cubic (Wyckoff)
Lattice parameters of AlMg	Lattice parameters of Al-Fe-
Phase: $a = b = c = 4.0542(1)$	Ni Phase: $a = b = c = 4.599(7)$
\AA , $\alpha = \beta = \gamma = 90^\circ$	\AA , $\alpha = \beta = \gamma = 90^\circ$
$V = 66.640(6) \text{\AA}^3$ and $\rho = 2.559 \text{ gr.cm}^{-3}$	$V = 66.92(3) \text{\AA}^3$ and $\rho = 3.222 \text{ gr.cm}^{-3}$

The refinement results show that the diffraction patterns of Al-Fe-Ni-Mg alloys heated for 1 hour, 2 hours, and 3 hours (shown in Figs 7, 8, and 9) have good fitting performance, with R and chi-square factors having relatively small numbers and remaining within the permissible value limit of about 1.254.

Furthermore, as shown in Fig. 9, the diffraction pattern of the Al-Fe-Ni-Mg alloy shows peaks of phase α at 2θ angles ranging from 22° , 24° , 43° , and 82° and peaks of phase θ at 2θ angles at 39° , 45° , 65° , 78° , and 82° . On the other hand, the diffraction pattern depicted in Fig. 8 demonstrates that the phase α and θ peaks that occur at 2θ angles typically coincide with the magnitude of the 2θ angle in the PDF and the outcomes of calculations using the BRAGG equation as shown in eq. 1. Moreover, there are 3 phase peaks in the α and θ phases but none in the phase κ . These findings indicate that the phases generated are composed of α and θ phases.

The phases α , θ , and κ represent Al, Fe-Al₃, and Ni-Al₃, respectively. Fe and aluminum react, and this reaction leads to the formation of phase θ . This reaction happens due to the phase α structure rejecting aluminum solid solutions that are more soluble in solids. The phase α structure is rejected because the Fe atoms' solubility has exceeded the 0.04% Fe limit, causing aluminum to react and bind the Fe to form Fe-Al₃ compounds.

Fig. 10 depicts the Al-Fe-Ni-Mg alloy's microstructure after three hours of 500°C heating. At 2,000 times magnification, the image demonstrates that the Al-Fe-Ni-Mg alloy's microstructure mainly consists of two-color regions, one dark and one light, with equiaxial grain shapes. In this instance, the x phase is represented by the light-colored areas, while the dark-colored regions represent the x phase and the metal compound phase. The Fe-Al₃ compound may be recognized as the y phase for newly created metal phase compounds.

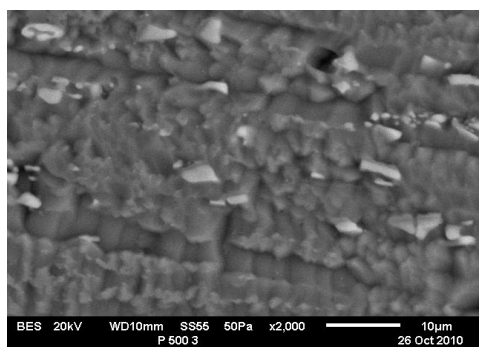


Fig. 10 Topography of the Al-Fe-Ni-Mg alloy microstructure using SEM

According to qualitative and semi-quantitative EDS analysis, the Al-Fe-Ni-Mg alloy's light and dark colors both

contain the components Al, Fe, Ni, and Mg, as illustrated in Fig. 11. Semi-quantitative analysis of the point's area shows that the percentages of Al, Fe, and Ni are approximately 81.05%, 4.24%, 7.23%, and 1.31%, respectively. As a result of these conditions, compound metals known as Fe-Al₃, NiAl₃, and FeNiAl₉ may form in the θ , κ , and τ phases, respectively [28].

The grain microstructure after heat treatment is depicted in Fig. 12 and Table 8, where it underwent a recrystallization process that made the grain structure equiaxial and tended to reduce its mechanical properties. The microstructure that tends to grow after three hours of heating is also shown in Fig. 12. Reduced hardness features result from enlarging microstructures. The mechanism of grain enlargement produces fewer grain boundaries. Thus, the barrier to dislocation movement is lowered, as well as the dislocation density [28], [29], [30], which causes a decline in the material's hardness properties.

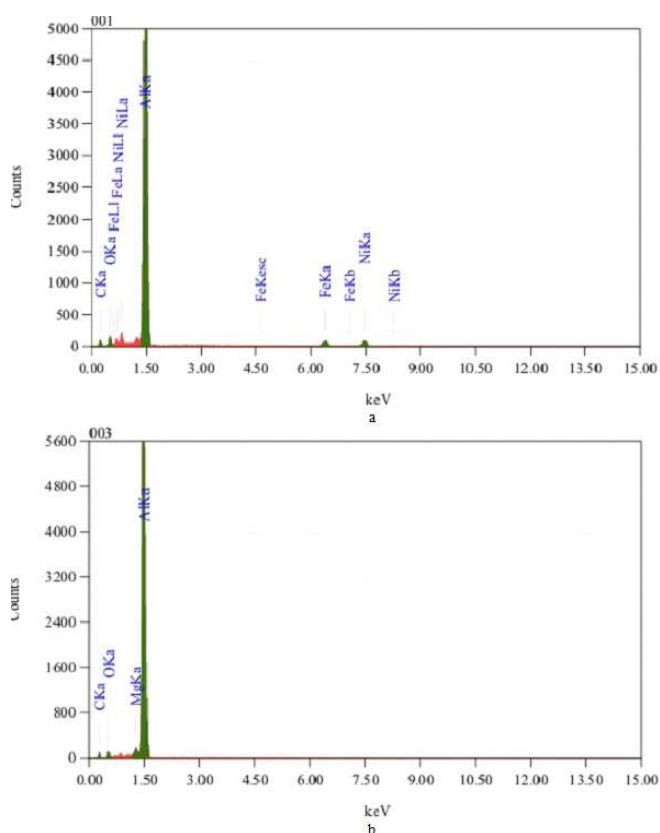


Fig. 11 EDS spectrum of stoichiometric Al-Fe-Ni-Mg alloy, a) in the bright (white) region, b) in the dark (gray) region.

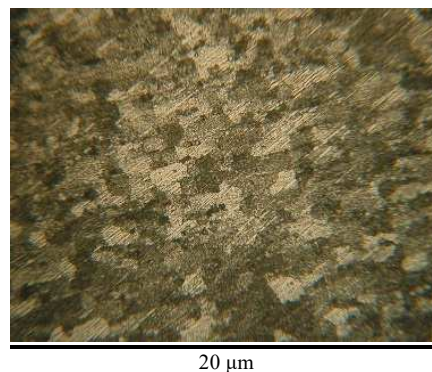


Fig. 12 Grain microstructure of Al-Fe-Ni-Mg after 3- hours heat treatment

TABLE VIII
AL-FE-NI-MG ALLOY CHARACTERISTICS

Characteristics	Deformed Al-Fe-Ni-Mg	Al-Fe-Ni-Mg after heat treatment
Grain structure	Elongated	Equiaxial
Mechanical properties, HV	163	86
Chi square	1,254	1,254

IV. CONCLUSION

The Al-Fe-Ni-Mg alloy has a cubic structure in the form of the (Al) phase, and the atoms of magnesium, iron, and nickel are all soluble in a condition of substitutional solid solution. The lattice parameters changed, indicating the formation of a solid solution phase that dissolved the solid Al-Mg and Al-Fe-Ni. Furthermore, it allows forming compound metals known as Fe-Al₃ metal compounds. The deformation process causes the topography of the grain structure with crystal orientation to have a tendency towards an elongated shape followed by an increase in hardness. On the other hand, Heat treatment caused the grain structure to change from an elongated to an equiaxial shape, followed by a reduction in hardness.

AUTHOR CONTRIBUTION

M. Husna Al Hasa, Wisnu Ariadi, Masrukan, Kemal Maulana Alhasa, Usman Sujadi, and Ratih Langenati contributed equally to this paper. All authors read and approved the final paper.

ACKNOWLEDGMENTS

We thank the Research Center for Nuclear Fuel Cycles and Radioactive Waste Technology (BRIN) for funding this research.

REFERENCES

- [1] M. X. Milagre et al., "Effects of Picture Frame Technique (PFT) on the corrosion behavior of 6061 aluminum alloy," *Journal of Nuclear Materials*, vol. 539, p. 152320, Oct. 2020, doi:10.1016/j.jnucmat.2020.152320.
- [2] Y. S. Kim, H. T. Chae, S. Van den Berghe, A. Leenaers, V. Kuzminov, and A. M. Yacout, "Aluminum cladding oxide growth prediction for high flux research reactors," *Journal of Nuclear Materials*, vol. 529, p. 151926, Feb. 2020, doi: 10.1016/j.jnucmat.2019.151926.
- [3] M. H. A. Hasa, Masrukan, and A. S. Adhi, "Materials Development and Hardness Properties of Aluminum Alloy," *Applied Mechanics and Materials*, vol. 575, pp. 83–87, Jun. 2014, doi:10.4028/www.scientific.net/amm.575.83.
- [4] X. Qi, Y. He, B. Jiang, and R. Song, "Effect of deformation and annealing on microstructure and corrosion behavior of 7075 aluminum alloy with micro arc oxidation coating," *Surface and Coatings Technology*, vol. 469, p. 129791, Sep. 2023, doi:10.1016/j.surfcoat.2023.129791.
- [5] X. Wang, M. Guo, W. Peng, Y. Wang, and L. Zhuang, "Relationship among solution heating rate, mechanical properties, microstructure and texture of Al–Mg–Si–Cu alloy," *Transactions of Nonferrous Metals Society of China*, vol. 31, no. 1, pp. 36–52, Jan. 2021, doi:10.1016/s1003-6326(20)65477-2.
- [6] A. Ghosh, A. Roy, A. Ghosh, and M. Ghosh, "Influence of temperature on microstructure, crystallographic texture and mechanical properties of EN AW 6016 alloy during plane strain compression," *Materials Today Communications*, vol. 26, p. 101808, Mar. 2021, doi:10.1016/j.mtcomm.2020.101808.
- [7] G. Inden, *Phase Equilibria in Iron Ternary Alloys*. By G. V. Raynor and V. G. Rivlin. The Institute of Metals, London 1988. xiii, 485 pp.,

- bound, US \$ 129.—ISBN 0-901462-34-9, *Adv. Mater.*, 1990, 2(1), p 58–59.
- [8] Y. Sun, K. Zhang, and G. Gong, "Material properties of structural aluminum alloys after exposure to fire," *Structures*, vol. 55, pp. 2105–2111, Sep. 2023, doi: 10.1016/j.istruc.2023.07.027.
- [9] E. Perez-Badillo, H. Dorantes-Rosales, M. Saucedo-Muñoz, and V. Lopez-Hirata, "Analysis of Phase Transformations in Fe-Ni-Al Alloys Using Diffusion Couples of Fe/Fe-33at.%Ni-33at.%Al Alloy/Ni," *Metals*, vol. 13, no. 7, p. 1221, Jul. 2023, doi: 10.3390/met13071221.
- [10] L. F. Mondolfo, "Aluminum Alloys: Structure and Properties" (Butterworths, London-Boston, 1976) p. 566.
- [11] American Society for Testing and Materials Annual, "Annual Book of ASTM Standards," vol. Sec., 4. 1992.
- [12] P. Zhang, J. Liu, Y. Gao, Z. Liu, and Q. Mai, "Effect of heat treatment process on the micro machinability of 7075 aluminum alloy," *Vacuum*, vol. 207, p. 111574, Jan. 2023, doi:10.1016/j.vacuum.2022.111574.
- [13] Z. Bian et al., "Coarsening behavior of Al3Sc interface precipitates and related impact on mechanical properties of AlFeNi-Sc alloy at 400 °C," *Materials Science and Engineering: A*, vol. 877, p. 145189, Jun. 2023, doi: 10.1016/j.msea.2023.145189.
- [14] M. Wintergerst, N. Dacheux, F. Datchary, E. Herms, and B. Kapusta, "Corrosion of the AlFeNi alloy used for the fuel cladding in the Jules Horowitz research reactor," *Journal of Nuclear Materials*, vol. 393, no. 3, pp. 369–380, Sep. 2009, doi: 10.1016/j.jnucmat.2009.06.003.
- [15] Izumi, F.A. "Rietveld-refinement program RIETAN-94 for angle-dispersive X-ray and neutron powder diffraction", National Institute for Research in Inorganic Materials, Japan, 1997, 35 P.
- [16] R. W. Wyckoff, "Crystal Structure," Second., New York: Interscience Publishers, 1963.
- [17] Z. Bian et al., "Thermal stability of Al–Fe–Ni alloy at high temperatures," *Journal of Materials Research and Technology*, vol. 8, no. 3, pp. 2538–2548, May 2019, doi: 10.1016/j.jmrt.2019.01.028.
- [18] Z. Bian et al., "Regulating microstructures and mechanical properties of Al–Fe–Ni alloys," *Progress in Natural Science: Materials International*, vol. 30, no. 1, pp. 54–62, Feb. 2020, doi:10.1016/j.pnsc.2019.12.006.
- [19] Z. Bian et al., "Coupling analysis on controlling mechanisms for creep of Al-Fe-Ni alloy," *Transactions of Nonferrous Metals Society of China*, vol. 33, no. 5, pp. 1331–1344, May 2023, doi: 10.1016/s1003-6326(23)66186-2.
- [20] P. Sun et al., "The effect of rolling temperature on the microstructure and properties of multi pass rolled 7A04 aluminum alloy," *Journal of Materials Research and Technology*, vol. 25, pp. 3200–3211, Jul. 2023, doi: 10.1016/j.jmrt.2023.06.123.
- [21] S. J. Yao et al., "Microstructural characterization and mechanical properties of 6061 aluminum alloy processed with short-time solid solution and aging treatment," *Journal of Alloys and Compounds*, vol. 960, p. 170704, Oct. 2023, doi: 10.1016/j.jallcom.2023.170704.
- [22] E. Kabliman, A. H. Kolody, J. Kronsteiner, M. Kommenda, and G. Kronberger, "Application of symbolic regression for constitutive modeling of plastic deformation," *Applications in Engineering Science*, vol. 6, p. 100052, Jun. 2021, doi:10.1016/j.apples.2021.100052.
- [23] J.-P. Brüggemann et al., "Structural optimization of a wheel force transducer component for more realistic acquisition of vehicle load data and fracture mechanical evaluation," *Applications in Engineering Science*, vol. 5, p. 100032, Mar. 2021, doi:10.1016/j.apples.2020.100032.
- [24] J. Setiawan, S. Pribadi, G. K. Suryaman, and M. H. A. Hasa, "Structural analysis on in situ high-temperature XRD of corundum," *Proceedings of the 4th International Seminar on Metallurgy and Materials (ISMM2020): Accelerating Research and Innovation on Metallurgy and Materials for Inclusive and Sustainable Industry*, 2021, doi: 10.1063/5.0059971.
- [25] J. Setiawan, S. Pribadi, A. Jamaludin, Sungkono, and M. H. Al Hasa, "Structural analysis of Al alloys for nuclear fuel cladding," *1st International Seminar on Advances In Metallurgy and Materials (i-SENAMM 2019)*, 2020, doi: 10.1063/5.0015710.
- [26] J. Setiawan, P. Slamet, J. Agus, M. H. Al Hasa, and H. P. Djoko, "Phase Composition of Sintered AlCrFeNi," in *Key Engineering Materials*, 2022, vol. 908 KEM, pp. 457–461.
- [27] M. Masrukan, M. H. Al Hasa, and E. Yusnitha, "Fabrication of fuel element core (FEC) of U–6Zr–5Nb/Al to be fuel element plate (FEP) with variation of uranium density," *Journal of Materials Research and Technology*, vol. 10, pp. 216–224, Jan. 2021, doi:10.1016/j.jmrt.2020.11.110.

- [28] Y. Hongfu et al., "Effect of rolling deformation and passes on microstructure and mechanical properties of 7075 aluminum alloy," *Ceramics International*, vol. 49, no. 1, pp. 1165–1177, Jan. 2023, doi:10.1016/j.ceramint.2022.09.093.
- [29] M. M, M. H. Alhasa, and S. Octa D, "Analysis of Chemical and Phase Composition in Powder of U-Zr-Nb Post Hydriding-Dehydriding Process," *International Journal on Advanced Science, Engineering and Information Technology*, vol. 12, no. 1, p. 347, Jan. 2022, doi: 10.18517/ijaseit.12.1.11241.
- [30] X. Yin et al., "Thermal stability, microstructure evolution and grain growth kinetics of ultrafine grained Al 7075 alloy processed by cryogenic temperature extrusion machining," *Journal of Alloys and Compounds*, vol. 950, p. 169900, Jul. 2023, doi:10.1016/j.jallcom.2023.169900.